Dielectrophoresis Driven Spreading of Immersed Liquid Droplets

Carl V. Brown * (1), Glen McHale (2), and Christophe L. Trabi (1, 2)

(1) Nottingham Trent University, School of Science & Technology, Clifton Lane, Nottingham NG11 8NS, UK

(2) Northumbria University, Faculty of Engineering & Environment, Ellison Place, Newcastle upon Tyne NE1 8ST, UK

* Author for correspondence carl.brown@ntu.ac.uk

Abstract

Non-wetting oleophobic surfaces can be forcibly wetted by using non-uniform electric fields and an interface-localized form of liquid dielectrophoresis. Here we show that this effect can be used to create films of oil immersed in a second immiscible fluid of lower permittivity. We predict that the square of the thickness of the film should obey a simple law dependent on the square of the applied voltage and with strength dependent on the ratio of difference in permittivity to the liquid-fluid interfacial tension, $\Delta\varepsilon/\gamma_{LF}$. This relationship is experimentally confirmed for liquid-air and liquid-liquid combinations with $\Delta\varepsilon/\gamma_{LF}$ having a span of more than two orders of magnitude.

Introduction

Controlling the wetting of liquids on surfaces can be achieved by modifying materials properties, *via* surface chemistry modification [1] or the use of surfactants [2], the use of surface texture to amplify surface chemistry induced tendencies, such as in superhydrophobicity [3, 4], or a combination of surface texture and liquid infusion, such as in slippery liquid-infused porous surfaces [5]. An alternative approach used in electrowetting, which provides active control, is to use an applied voltage to control the balance between the various interfacial energies and the capacitive energy resulting from the contact between a conducting droplet and an electrically insulating layer on a conducting contact [6, 7]. This approach has proven effective in creating liquid lenses [8], liquid paper [9] and in microfluidic systems [10,11]. A critical aspect has been to do so in liquid-in-liquid systems because of the need to remove the effects of gravity through neutral buoyancy, safeguard against impact shocks, or to encapsulate a liquid which might otherwise evaporate.

A fundamental limitation of electrowetting is that although droplets can be made more wetting they cannot be induced into films irrespective of whether they are in air or immersed in a second liquid [12]. In contrast, liquid dielectrophoresis [13] can be used to induce partial wetting of droplets and to create dielectric liquid lenses [14, 15, 16]. Recently, we have elucidated the principles of dielectrowetting [17], an interface-localized form of liquid dielectrophoresis which can be used to create films. It has been shown how it can be used to create voltage programmable diffraction gratings [18], optical shutters [16, 19, 20] or induce voltage-controlled super-spreading in air [21]. In this report, we develop a theoretical model of the dielectrowetting induced formation of films of one liquid immersed in a second immiscible fluid (air or liquid) that has a lower dielectric constant and show its experimental validity for a range of different combinations of stripe-shaped droplets in fluids of lower dielectric constant. In so doing, we provide a new approach to enable liquid-liquid interfacial tensions to be measured.

Experimental

Experiments were performed on liquid droplets resting on a borosilicate glass slide substrate whilst immersed in either air or in another immiscible liquid. A photograph and a schematic diagram of the experimental geometry are shown in Fig. 1(a) and Fig. 1(b) respectively. The substrate was pre-coated with a 25 nm layer of indium tin oxide of resistivity 100 Ohm/square (Praezisions Glas and Optik GmbH, Iserlohn, Germany). On the substrate was an array of co-planar interdigital stripe electrodes for which both the electrode linewidths and the gaps between the electrodes were the same, d = 80 μm. The electrode pattern was produced using standard photolithographic procedures. The electrodes were coated with a 0.7 μm capping layer of photoresist (SU8-10, MicroChem Corp., Newton, MA, USA) which was oxidized in a UV/Ozone ProCleaner (Bioforce Nanoscience Inc., Ames, IA, USA) for 20 min. The substrate was finally treated with a commercial hydrophobic preparation (Granger's Extreme Wash-in, Grangers International Ltd, Alfreton, Derbyshire UK) diluted to 1:20 by volume in deionised water. This provides a thin dielectric layer with a smooth surface that provides resistance to electrical breakdown.

Figs. 1(b) and 1(c) show the side and top views respectively of a static droplet of propylene glycol immersed in decane whilst different a.c. voltages are applied to one set of electrode fingers with the inter-posed fingers maintained at earth potential. The surrounding decane liquid was contained in a cuvette, with a removable lid to prevent liquid evaporation. This was sealed onto the substrate using UV cured epoxy adhesive. The droplet was dispensed under the decane onto the electrode area of the substrate using a volume-calibrated "Gilson Pipetman" micropipette (Gilson, Inc., Middleton, USA). Electrical addressing of the device was performed with a 10 kHz sinewave voltage provided by a wave form generator connected to a PZD700A-1 amplifier (Trek Inc., Medina, New York, USA). The voltage was increased quasi-statically with 60 seconds between voltage increments to avoid entrainment of decane between the spread film of propylene glycol and the electrodes. Images of the

immersed droplet were recorded using a standard USB video camera (DCC1645C, ThorLabs, Ely, UK) fitted with a 10× objective lens.

With no applied voltage (labelled 0 V) the droplet forms a spherical cap, appearing as a circular arc with a contact angle of 125° viewed from the sides, i.e. from the *x*-direction and from the y-direction shown in Fig. 2(a) and in Fig. 2(b) respectively, and as a circular outline viewed from the top (*z*-direction) in Fig. 2(c). When the voltage is raised to 100 V (r.m.s.) the droplet adjusts position slightly in the *x*-*y* plane so that its upper and lower edges in the *x*-direction both tend to lie above gaps between electrodes rather than electrodes, its height *h* decreases, and its contact angle reduces to 110°, as shown in Fig. 2(a). The droplet begins to elongate in the y-direction and its outline in Fig. 2(c) is no longer circular. At still higher voltages, 150 V and 200 V, the droplet continues to flatten and reduce its height *h* in the *z*-direction, whilst its length *l* in the *y*-direction increases. At these voltages Fig. 2(a) and Fig. 2(b) show that the side profile, viewed from both the x-direction and from the y-directions, deviates from a circular arc. Interestingly, the local contact angle viewed orthogonal to the direction of spreading, i.e. from the x-direction, is maintained at a value that remains near to 90°, as shown in the contrast enhanced magnified image of the region near to the contact line in the direction of spreading at 200 V in Fig. 2(a). A saturation of a local contact angle has also been observed to occur at the higher voltages in electrowetting within the characteristic length-scale governing the capacitive energy of the system, i.e. the thickness of the dielectric [22]. Here for dielectrowetting the equivalent length-scale, the distance between electrodes, is larger.

Figs. 2(b) and 2(c) show that whilst spreading in the y-direction occurs, the width w in the x-direction remains constant as a result of the electrode symmetry in our system. The electrodes form parallel stripes in the y-direction, giving rise to a potential that is spatially varying only in one direction, the x-direction. The electrostatic energy of the system is reduced when the regions of high electric field intensity between the electrodes are occupied by a material that is highly polarisable, here the liquid with higher dielectric constant. The force to actuate

liquid movement into these regions is provided via its interaction with the highly non-uniform fringing electric fields occurring in the regions close to both edges of the electrodes [23] [24]. These forces depend on the square of the gradient in the electric field and hence direct the liquid towards the electrode gaps in the x-direction, but away from the lower electric field regions above the electrodes themselves. This gives rise to an effective electrostatic barrier to the liquid spreading across the regions above electrodes, and acts to maintain the width of a spreading droplet to be equal to an integer number of electrode gaps.

Results and discussion

The height h and the length l of the droplet of propylene glycol immersed in decane are plotted as a function of magnitude of the applied voltage in Fig. 3. Although the values of h and l remained similar below 50 V, the values begin to diverge at 60 V and above with the length increasing and the droplet height decreasing as the droplet spreads in the y-direction and flattens. Above 100 V we observed that the product of these quantities, $\Omega = h \cdot l$, shown in Fig. 2 by the filled circles, remained relatively constant and within the range $(0.59 \pm 0.04) \times 10^{-6}$ m^2 as the voltage was increased to 210 V. This observation, along with the flattened non-circular shapes shown during spreading at high voltages in Fig. 2(c), prompted us to adopt the rectangular cuboid model geometry in Fig. 3(l) to develop a theoretical model of quasi-static dielectrophoresis driven spreading based on the balance between interfacial energies and dielectrophoretic energies.

There are five interfaces between the cuboidal rectangular liquid droplet and the fluid in which it is immersed and these give a contribution to the total interfacial energy, W_S, of $[(l+2h)w + 2hl]\gamma_{LF}$, where γ_{LF} is the liquid-fluid interfacial tension. There are also contributions from the solid-liquid interface, $lw\gamma_{SL}$, and the solid-fluid interface, $(l_\infty - l)w\gamma_{SF}$, where γ_{SL} and γ_{SF} are the solid-liquid and solid-fluid interfacial tensions and l_∞ is the length of the solid surface in the y-direction. Writing the cross-sectional area of the droplet as $\Omega = hl$, which is constant, gives the following expression for the total interfacial energy:

$$W_S = w\left(\frac{\Omega}{h} + 2h\right)\gamma_{LF} + w\frac{\Omega}{h}(\gamma_{SL} - \gamma_{SF}) + 2\Omega\gamma_{LF} + wl_\infty\gamma_{SF} \quad (1)$$

This can be minimised with respect to the droplet height h, taking into account the constant width w, and hence re-written in terms of a zero voltage equilibrium height h_o,

$$W_S = 2wh\left(1 + \frac{h_o^2}{h^2}\right)\gamma_{LF} + wl_\infty\gamma_{SF} + 2\Omega\gamma_{LF} \quad (2)$$

where $h_o^2 = [1 + (\gamma_{SL}-\gamma_{SF})/\gamma_{LF}]\Omega/2$, which can be written $h_o^2 = [1 - \cos\theta_e]\Omega/2$ using the combination of interfacial tensions to define an equivalent Young's law contact angle for an immersed droplet.

When a dielectric fluid of permittivity ε is in contact with a substrate having interdigitated electrodes to which a voltage $V(x) = V_o\cos(\frac{1}{2}\pi x/d)$ is applied, then an exponentially decaying electric field penetrates into the fluid and electrostatic energy, W_E, is stored. A two dimensional solution to the Maxwell equation $\underline{\nabla}\cdot\underline{\mathbf{D}} = 0$ gives $V(x, z) = V_o\cos(2x/\delta)\exp(-2z/\delta)$ where $\delta = 4d/\pi$ has been defined as a penetration depth and is determined by the periodicity of the electrodes. Integrating the electrostatic energy per unit area in the x-y plane and assuming the fluid thickness is much greater than the decay length gives $W_E = -\frac{1}{2}(\varepsilon_o\varepsilon V_o^2/\delta)$ [17]. In the region above the electrodes which is covered only by the immersing fluid, $-w/2 < x < w/2$, $-\infty < y < -l/2$ and $l/2 < y < \infty$, this gives the first term in the electrostatic contribution to the total energy,

$$W_E = -\frac{\varepsilon_o\varepsilon_F V_{o.}^2}{2\delta}\left(l_\infty - \frac{\Omega}{h}\right)w - \frac{\varepsilon_o\varepsilon_L V_{o.}^2}{2\delta}g\left(h/d, \varepsilon_L, \varepsilon_F\right)\frac{\Omega}{h}w \quad (3)$$

The electrode region $-w/2 < x < w/2$, $-l/2 < y < l/2$, is covered by a liquid droplet and there is an interface between the liquid and the immersing fluid at $z = h$. A model can be constructed

with two fluid layers and solving Maxwell's equations with appropriate boundary conditions at each interface. The second term in Eq. 3 gives the analytical approximation for the electrostatic energy in this situation using the first two Fourier modes to describe the spatially periodic potential [25], where the factor $g\left(h/d,\varepsilon_L,\varepsilon_F\right)$ is given by:

$$g\left(h/d,\varepsilon_L,\varepsilon_F\right)=\frac{\left(1-\frac{\left(\varepsilon_L-\varepsilon_F\right)}{\left(\varepsilon_L+\varepsilon_F\right)}\exp\left(-\frac{\pi h}{d}\right)\right)}{\left(1+\frac{\left(\varepsilon_L-\varepsilon_F\right)}{\left(\varepsilon_L+\varepsilon_F\right)}\exp\left(-\frac{\pi h}{d}\right)\right)} \tag{4}$$

This factor can be approximated to unity provided that the spread film thickness *h* remains significantly larger than the electrode gap *d*. The expression for the total energy, $W_T = W_S + W_E$, is then given by,

$$W_T=2wh\left(1+\frac{h_o^2}{h^2}\right)\gamma_{LF}+wl_\infty\gamma_{SF}+2\Omega\gamma_{LF}-\frac{\varepsilon_o\varepsilon_F V_{o.}^2}{2\delta}\left(l_\infty-\frac{\Omega}{h}\right)w-\frac{\varepsilon_o\varepsilon_L V_{o.}^2}{2\delta}\frac{\Omega}{h}w \tag{5}$$

The voltage dependent height is then given by minimising the total energy $W_T = W_S + W_E$ with respect to the droplet height *h*,

$$h^2\left(V_o\right)=h_o^2-\frac{\varepsilon_o\Delta\varepsilon V_{o.}^2\Omega}{4\delta\gamma_{LF}} \tag{6}$$

where $\Delta\varepsilon = (\varepsilon_L - \varepsilon_F)$ is the contrast in relative permittivity between the fluid and the droplet. Equation 6 predicts that on a given substrate a stripe droplet spreading due to dielectrowetting as a rectangular cuboid of constant width will reduce the square of its thickness in proportion to the square of the applied voltage with a gradient proportional to $\Delta\varepsilon/\gamma_{LF}$. ~~Thus, if the contrast in permittivity is known the liquid-fluid interfacial tension can be calculated~~.

Previous reports of the use of dielectric forces for optofluidics have tended to employ circular electrode geometries to promote axially symmetric immersed droplet actuation [15] [16]. In the form used they rise to non-uniform dielectric forces that strongly vary with radius and so these geometries are not so readily accessible to such an analytical theoretical approach to describing the dependence of the wetting on the voltage.

To test the effectiveness of Eq. 6 further we performed a systematic series of experiments using droplets of hexadecane, 1-decanol, trimethylolpropane triglycidyl ether (TMPGE), propylene glycol and propylene carbonate with relative permittivity ε_L = 2.05, 7.93, 12.7, 27.5, 66.1, respectively in air, hexadecane, dodecane, decane, hexane and hexadecane with ε_F = 1.0, 2.05, 2.01, 1.99, 1.89 and 2.05, respectively (Table I). We used pendant drop measurements (Drop shape analysis, A. Krüss Optronic GmbH, Hamburg, Germany) to obtain the liquid-fluid interfacial tensions and these ranged from (5.3 ± 0.1) mJ m^{-2} to (40.9 ± 0.3) mJ m^{-2}. The equilibrium contact angles at zero voltage, θ_e(V = 0), for each of the immersed liquid droplets that were studied in the experiments are also given in table I. The liquid-fluid combinations used spanned a range of more than two orders of magnitude of $\Delta\varepsilon/\gamma_{LF}$ from (38.7 ± 0.3) J^{-1} m^2 to (5900 ± 100) J^{-1} m^2. Figs. 4(a)-(k) show the measured value of h^2/Ω plotted against the square of the r.m.s. value of the voltage, which is half the peak voltage V_o, because our AC voltage is applied to every other electrode with the interposed electrodes at earth potential. In several cases there is a clear hysteresis, an initial centering of the droplet on the set of electrodes at the lower voltages, before spreading in a rectangular cuboid shape occurs and the linear relationship between h^2/Ω and V_{rms}^2 then obtains only at the higher voltages. Interestingly, for some of the liquid/fluid combinations in Fig. 3, especially those liquid/fluid combinations with smaller values of the parameter $\Delta\varepsilon/\gamma_{LF}$, the data do appear to also fall onto the same linear fit for the whole range of the voltages shown.

For the range of liquid-air and liquid-liquid combinations given in Table I the factor $g(h/d, \varepsilon_L, \varepsilon_F)$ defined in Eq. 4 only drops to below 0.99 when $h < 1.68d$ for $\Delta\varepsilon$ = 65.1, and when $h < 1.35d$ for $\Delta\varepsilon$ = 1.05. This is not significant in the voltage range where the spread

film thickness h remains significantly larger than the electrode gap d as is the case where the linear relationships apply in Fig. 4.

According to Eq. 6 the gradient m of each plot should be directly proportional to the ratio of the materials parameters, $\Delta\varepsilon/\gamma_{LF}$, where the coefficient of proportionality (given how the voltage is applied in the experiment) is predicted to be $(\varepsilon_0/16\delta)=5.43\times10^{-9}$ $JV^{-2}m^{-2}$. This is in excellent agreement with the data summarized in Fig. 5 which has an experimentally determined value of $(5.6 \pm 0.1) \times 10^{-9}$ $JV^{-2}m^{-2}$.

Equation 6 implies that there would be an extrapolated voltage at which the film thickness would be zero. The mathematical form of equation 6 results from making the assumption that $g(h/d, \varepsilon_L, \varepsilon_F) = 1$. In reality, however, $g(h/d, \varepsilon_L, \varepsilon_F)$ deviates from unity as the film thickness decreases and the height of the liquid/fluid interface above the substrate comes down to within the penetration length δ. In this higher voltage regime we would expect a wrinkle deformation to develop at the liquid/fluid interface with amplitude that increases as the voltage is further increased. We observed this wrinkling effect at relatively lower voltages in previous work [18] on dielectrophoresis induced spreading because we started from droplets with equilibrium contact angles $\theta_e(V = 0)$ that were significantly lower than used in the current work.

Summary and conclusion

Our measurements show that it is possible to quantitatively describe the liquid-dielectrophoresis induced spreading of a dielectric liquid droplet immersed in a second fluid. The excellent agreement between the data and theory suggests the value of $\Delta\varepsilon/\gamma_{LF}$ for a liquid with unknown properties for either the permittivity of one of the fluids or of the liquid-fluid interfacial tension could be determined in a simple manner. The principles of liquid-in-fluid dielectrowetting should be applicable to lossy dielectric liquids at higher frequencies, such as water [13]. Finally, the ability to perform dielectrowetting in liquid-in-liquid systems

with the potential for optical contrast provides the opportunity to develop applications where density matching to provide neutral buoyancy may be important, such as a shock resistant programmable diffraction grating.

Acknowledgments

The authors gratefully acknowledge the financial support of the UK EPSRC (Grants EP/K014803/1 and EP/E063489/1).

References

[1] A. W. Adamson and Gast. A.P., *Physical Chemistry of Surfaces*, 6th Ed. Wiley, New York, ISBN 0471148733 (1997)

[2] Ivanova, N.A., and Starov, V.M. , "Wetting of low free energy surfaces by aqueous surfactant solutions", *Curr. Opin. Colloid Interface Sci.* **16**(4), 285-291 (2011) http://dx.doi.org/10.1016/j.cocis.2011.06.008

[3] Quéré, D., "Wetting and roughness", *Annu. Rev. Mater. Res.* **38**, 71-99 (2008) http://dx.doi.org/10.1146/annurev.matsci.38.060407.132434

[4] Shirtcliffe, N.J., McHale, G., Atherton, S., and Newton, M.I., "An introduction to superhydrophobicity", *Adv. Colloid Interface Sci.* **161**, 124-138 (2010) http://dx.doi.org/10.1016/j.cis.2009.11.001

[5] Wong, T.-S., Kang, S.H., Tang, S.K.Y., Smythe, E.J., Hatton, B.D., Grinthal, A. and Aizenberg, J., "Bioinspired self-repairing slippery surfaces with pressure-stable omniphobicity", *Nature* **477**(7365), 443-447 (2011) http://dx.doi.org/10.1038/nature10447

[6] Berge, B. , "Electrocapillarity and Wetting of Insulator Films by water", *Comptes Rendus Acad. Sci. Ser. II* **317**(2), 157-163 (1993)

[7] Mugele, F., and Baret, J.-C., "Electrowetting: From basics to applications", *J. Phys. Condens. Matter* **17**(28), R705-R774 (2005) http://dx.doi.org/10.1088/0953-8984/17/28/R01

[8] Berge, B., and Peseux, J., "Variable focal lens controlled by an external voltage: An application of electrowetting", *Eur. Phys. J. E* **3**(2), 159-163 (2000) http://dx.doi.org/10.1007/s101890070029

[9] Hayes, R.A., and Feenstra, B.J., "Video-speed electronic paper based on electrowetting", *Nature* **425** (6956), 383-385 (2003) http://dx.doi.org/10.1038/nature01988

[10] Fair, R.B., "Digital microfluidics: is a true lab-on-a-chip possible?", *Microfluid. Nanofluidics* **3**(3), 245-281 (2007)

http://dx.doi.org/10.1007/s10404-007-0161-8

[11] Pollack, M.G., Pamula, V.K., Srinivasan, V., and Eckhardt, A.E., "Applications of electrowetting-based digital microfluidics in clinical diagnostics", *Expert Rev. Mol. Diagn.* **11**(4), 393-407 (2011)
http://dx.doi.org/10.1586/ERM.11.22

[12] Chevalliot, S., Kuiper, S., and Heikenfeld, J., Adhes, J. "Experimental Validation of the Invariance of Electrowetting Contact Angle Saturation", *Sci. Technol.* **26**(12), 1909-1930 (2012)
http://dx.doi.org/10.1163/156856111X599580

[13] Jones, T. B., Gunji, M., Washizu, M., and Feldman, M. J., "Dielectrophoretic liquid actuation and nanodroplet formation", *J. Appl. Phys.* **89**(2), 1441-1448 (2001)
http://dx.doi.org/10.1063/1.1332799

[14] Cheng, C.-C., Chang, C. A., and Yeh, J. A., "Variable focus dielectric liquid droplet lens", *Opt. Express* **14**(9), 4101-4106 (2006)
http://dx.doi.org/10.1364/OE.14.004101

[15] Yang, C.-C., Yang, L., Tsai, C. G., Jou, P. H., and Yeh, J.A, "Fully developed contact angle change of a droplet in liquid actuated by dielectric force", *Appl. Phys. Lett.* **101**(18), 182903 (2012)
http://dx.doi.org/10.1063/1.4759112

[16] Xu, S., Ren, H. and Wu, S.-T., "Dielectrophoretically tunable optofluidic devices", *J. Phys. D: Appl. Phys.* **46**(48), 483001 (2013)
http://dx.doi.org/10.1088/0022-3727/46/48/483001

[17] McHale, G., Brown, C. V., Newton, M. I., Wells, G. G., and Sampara, N., "Dielectrowetting Driven Spreading of Droplets", *Phys. Rev. Lett.* **107**(18), 186101 (2011)
http://dx.doi.org/10.1103/PhysRevLett.107.186101

[18] Brown, C. V., Wells, G. G., Newton, M. I., and McHale, G., "Voltage-programmable liquid optical interface", *Nat. Photonics* **3**(7), 403-405 (2009)
http://dx.doi.org/10.1038/NPHOTON.2009.99

[19] Zhao, R., Cumby, B., Russell, A., and Heikenfeld, J., "Large area and low power dielectrowetting optical shutter with local deterministic fluid film breakup", *Appl. Phys. Lett.* **103**(22), 223510 (2013) http://dx.doi.org/10.1063/1.4834095

[20] Russell, A., Kreit, E., and Heikenfeld, J., "Scaling Dielectrowetting Optical Shutters to Higher Resolution: Microfluidic and Optical Implications", *Langmuir* **30**(18), 5357-5362 (2014) http://dx.doi.org/10.1021/la5008582

[21] McHale, G., Brown, C. V., and Sampara, N., "Voltage-induced spreading and superspreading of liquids", *Nat. Commun.* **4**, 1605 (2013) http://dx.doi.org/10.1038/ncomms2619

[22] Buehrle, J. and Mugele, F., "Equilibrium drop surface profiles in electric fields", *J. Phys. Condens. Matter*, **19**(37), 375112 (2007) http://dx.doi.org/10.1088/0953-8984/19/37/375112

[23] Pohl, H. A., "Dielectrophoresis: The Behaviour of Neutral Matter in Non-Uniform Electric Fields", Cambridge Monographs on Physics, Cambridge University Press, Cambridge (1978)

[24] Lorrain, P., and Corson, D. R., "Electromagnetic Fields and Waves", 2nd ed. Freeman, San Francisco (1970)

[25] Brown, C. V., McHale, G., and Mottram, N. J., "Analysis of a static undulation on the surface of a thin dielectric liquid layer formed by dielectrophoresis forces", *J. Appl. Phys.* **110**(2), 024107 (2011) http://dx.doi.org/10.1063/1.3606435

Figure 1

(a) Photograph of the device used in the experiments, with the scale indicated by the vertical arrow, (b) Schematic diagram of the experimental geometry: a liquid droplet rests an array of interdigital electrodes whilst immersed in either air or in another immiscible liquid.

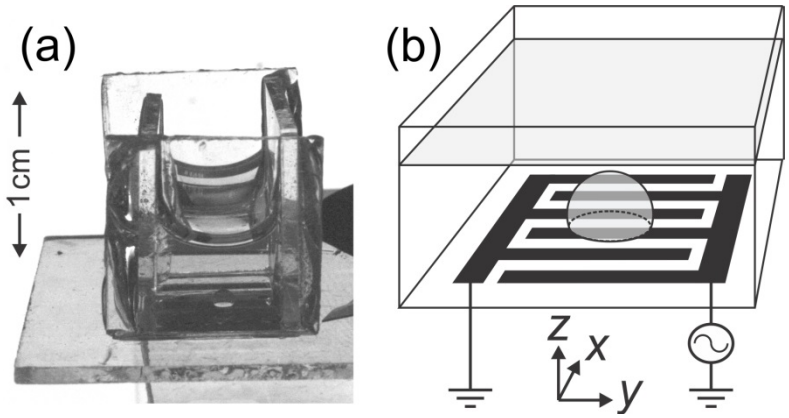

Figure 2

The shape of a droplet of propylene glycol immersed in decane is shown viewed (a) from the x-direction, (b) from the y-direction, and (c) from above, when different values of the a.c. sinewave voltage (r.m.s. values given) are applied to one set of electrode fingers.

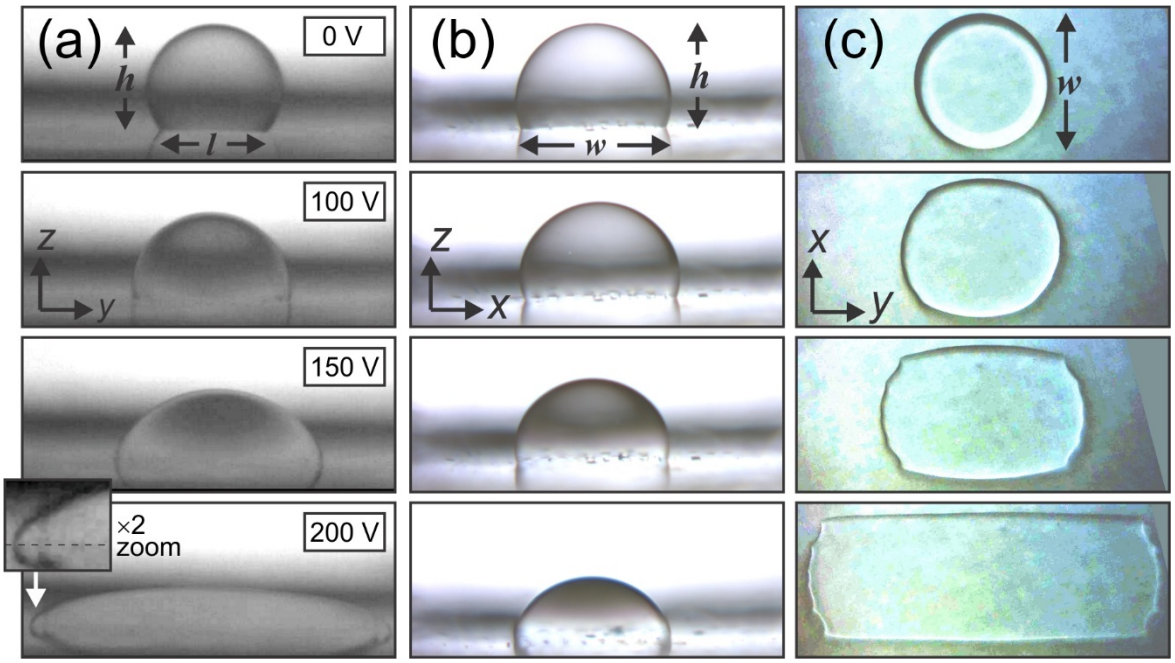

Figure 3

The height *h* (open diamonds) and the contact length *l* (open squares) values for the droplet of propylene glycol immersed in decane are plotted as a function of the r.m.s. value of the voltage applied to one set of electrode fingers. The values of *h* and *l* were measured from magnified images taken from the *x* direction, as defined in figure (1). The product of these quantities, $\Omega = h \times l$, shown by the filled circles, is also plotted as a function of voltage and using the right hand vertical axis scale.

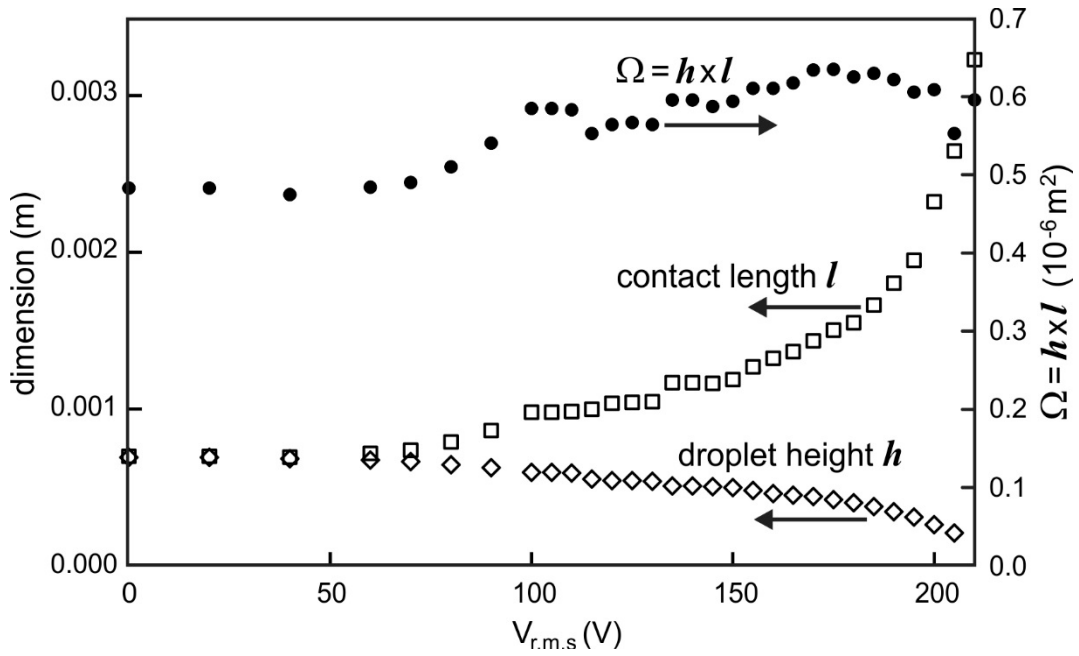

Table I

The different combinations of immersed liquid droplet and surrounding liquid/fluid that were used in the experiments.

Droplet		Immersion Fluid		Contact Angle $\theta_e(V = 0)$	Permittivity Difference $\Delta\varepsilon = \varepsilon_L - \varepsilon_F$	Interfacial tension γ_{LF} mJ m^{-2}	Ratio $(\Delta\varepsilon / \gamma_{LF})$ J^{-1} m^2
Liquid	ε_L	Fluid	ε_F				
hexadecane	2.05	air	1.00	76	1.05	27.1 ± 0.2	38.7 ± 0.3
1-decanol	7.93	air	1.00	87	6.93	28.5 ± 0.2	243 ± 2
TMPGE	12.7	air	1.00	74	11.7	40.5 ± 0.3	289 ± 2
propylene glycol	27.5	air	1.00	91	26.5	35.5 ± 0.3	747 ± 6
propylene carbonate	66.1	air	1.00	75	65.1	40.9 ± 0.3	1590 ± 10
TMPGE	12.7	hexadecane	2.05	88	10.6	5.3 ± 0.1	2000 ± 40
propylene glycol	27.5	hexadecane	2.05	113	25.5	9.9 ± 0.1	2580 ± 30
propylene glycol	27.5	dodecane	2.01	109	25.5	9.5 ± 0.1	2680 ± 30
propylene glycol	27.5	decane	1.99	116	25.5	9.5 ± 0.1	2680 ± 30
propylene glycol	27.5	hexane	1.89	111	25.6	7.4 ± 0.1	3460 ± 50
propylene carbonate	66.1	hexadecane	2.05	82	64.1	10.8 ± 0.2	5900 ± 100

Figure 4

Figures (a) to (k) show graphs of h^2/Ω (equivalently h/l) plotted against the square of the r.m.s. value of the voltage for each of the different combinations of immersed liquid droplet and surrounding fluid, either air or another liquid. In the higher voltage regions where the plots are linear a linear regression fit has been performed, shown by the solid lines. Figure (l) depicts the model geometry that was used in the theoretical analysis.

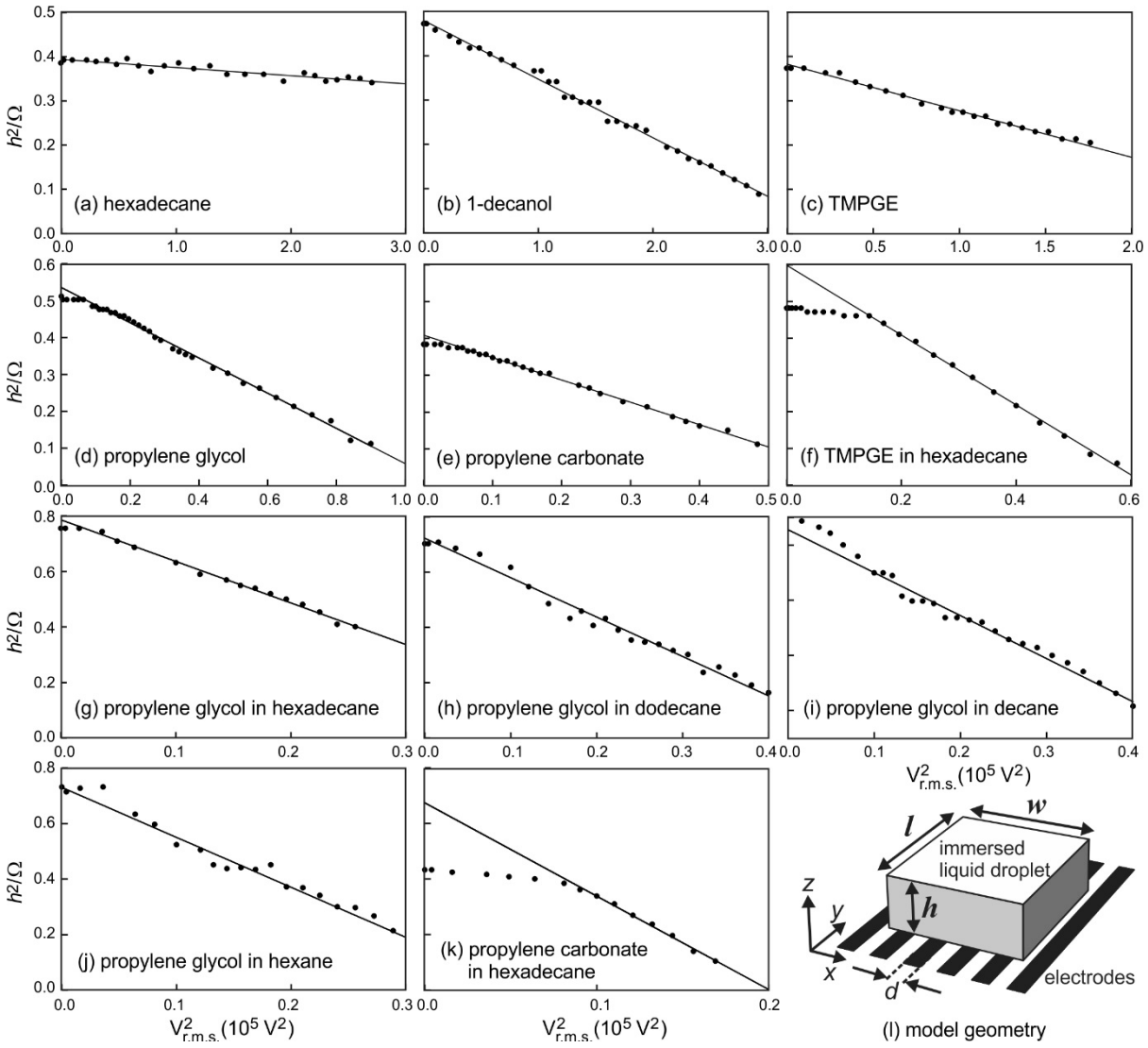

Figure 5

The gradients of the graphs in figures 3(a) to 3(k) (i.e. $h^2/\Omega = h/l$ versus the square of the r.m.s. voltage value) are plotted against the ratio ($\Delta\varepsilon/\gamma_{LF}$). Each data point, shown by the filled diamonds in the figure, is derived from data from one of the 11 different combinations of immersed liquid droplet and surrounding liquid/fluid used in the study. $\Delta\varepsilon = \varepsilon_F - \varepsilon_L$ is the difference between the permittivity of the immersed liquid and the permittivity of the surrounding liquid/fluid, and γ_{LF} is the interfacial surface tension for each combination, as shown in table 1.

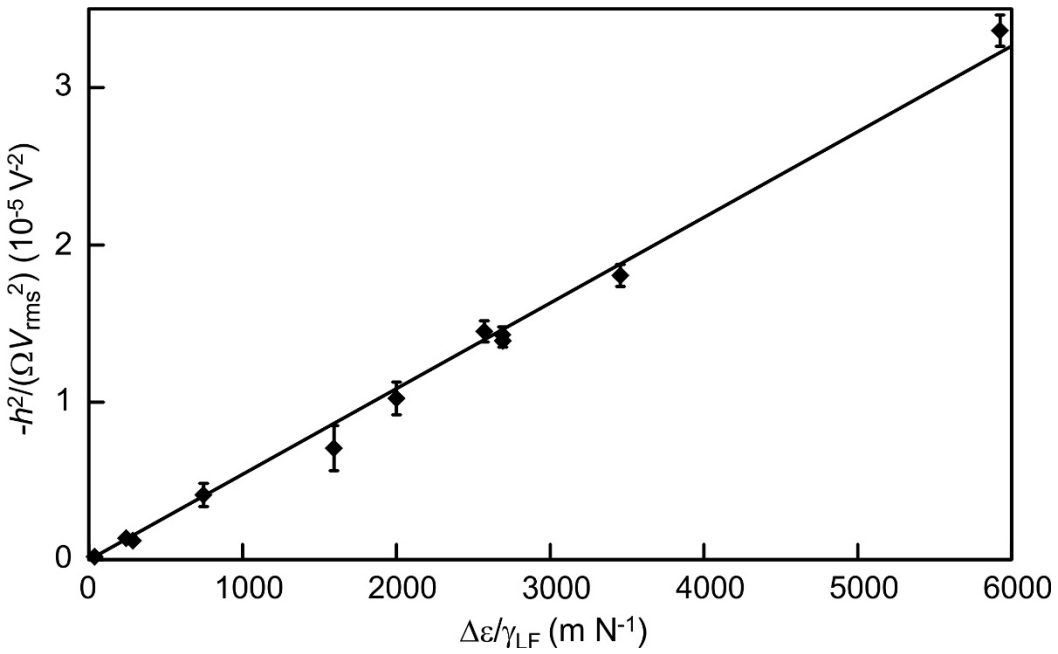

Table of Contents/Abstract Graphic